Enhancing 3D Reconstruction for Dynamic Scenes

Jisang Han[1*] **Honggyu An**[1*] **Jaewoo Jung**[1*] **Takuya Narihira**[2] **Junyoung Seo**[1]
Kazumi Fukuda[2] **Chaehyun Kim**[1] **Sunghwan Hong**[3] **Yuki Mitsufuji**[2,4†] **Seungryong Kim**[1†]

[1] KAIST AI [2] Sony AI [3] ETH Zürich AI Center, CVG, PRS [4] Sony Group Corporation

https://cvlab-kaist.github.io/DDUSt3R

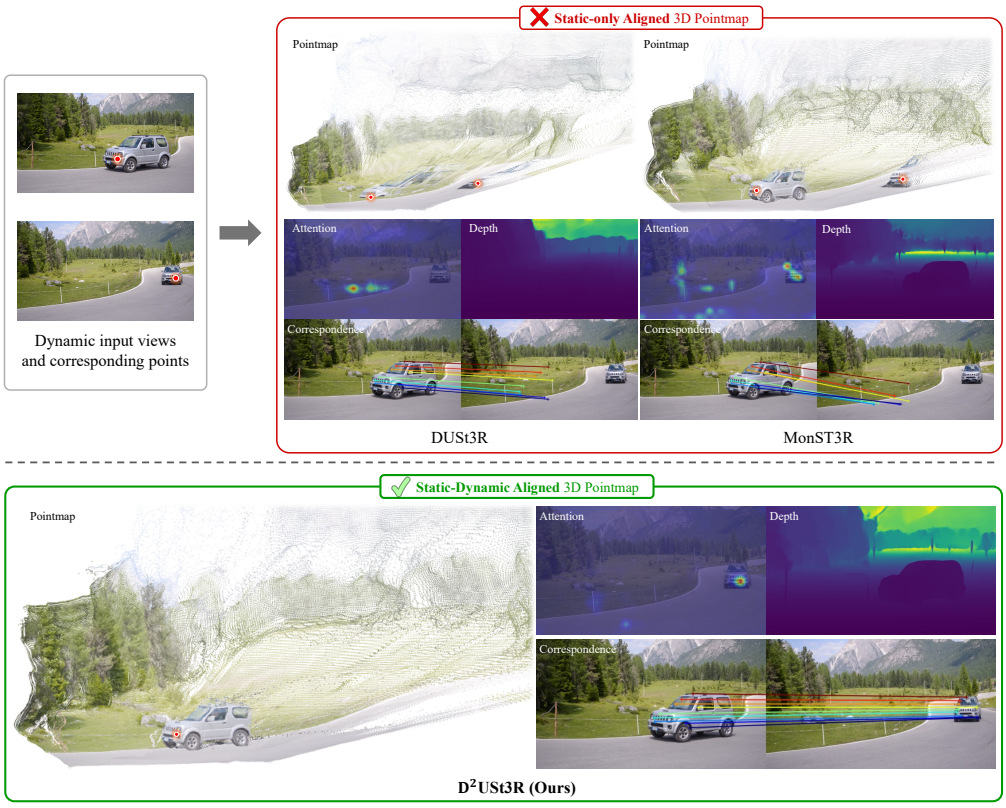

Figure 1: **Teaser.** Given a pair of input views, **D²USt3R** accurately establishes dense correspondence not only in static regions but also in dynamic regions, and enables 3D reconstruction of a dynamic scene via our proposed static-dynamic aligned pointmap. The colored • pointmaps highlight that DUSt3R [44] and MonST3R [51] align pointmaps solely based on camera motion, causing corresponding 2D pixels within dynamic object misaligned. We also compare the cross-attention maps, established correspondence fields, and estimated depth maps produced by **D²USt3R** against baseline methods [44, 51], where our method shows higher precision.

Abstract

In this work, we address the task of 3D reconstruction in dynamic scenes, where object motions frequently degrade the quality of previous 3D pointmap regression methods, such as DUSt3R, that are originally designed for static 3D scene reconstruction. Although these methods provide an elegant and powerful solution in static settings, they struggle in the presence of dynamic motions that disrupt alignment based solely on camera poses. To overcome this, we propose **D²USt3R** that directly regresses Static-Dynamic Aligned Pointmaps (SDAP) that simultaneously

39th Conference on Neural Information Processing Systems (NeurIPS 2025).

capture both static and dynamic 3D scene geometry. By explicitly incorporating both spatial and temporal aspects, our approach successfully encapsulates 3D dense correspondence to the proposed pointmaps, enhancing downstream tasks. Extensive experimental evaluations demonstrate that our proposed approach consistently achieves superior 3D reconstruction performance across various datasets featuring complex motions.

1 Introduction

Recovering 3D scene geometry from images remains a core problem in computer vision. Traditional approaches, such as Structure-from-Motion (SfM) [33] and Multi-View Stereo (MVS) [35], have achieved impressive results in this context. While these methods are originally designed for recovering precise 3D scene geometry, they often struggle with scenes that include objects, symmetries, imagery with minimal overlapping and textureless regions [26, 34, 3, 9].

To overcome these limitations, recent approaches [44, 21, 41] leverage a learning framework to streamline the 3D reconstruction pipeline and enhance performance. DUSt3R [44], as a pioneering method, introduced a unified learning-based framework for dense stereo 3D reconstruction. Specifically, DUSt3R directly regresses 3D pointmaps that encode scene geometry, pixel-to-scene correspondences, and inter-view relationships, mitigating error accumulation typical in multi-stage pipelines. Despite its strengths in static scenarios, DUSt3R significantly struggles with dynamic scenes due to its rigidity assumption, as exemplified in Figure 1.

Dynamic scenes, prevalent in real-world scenarios, pose significant challenges in 3D scene reconstruction task, as object motions disrupts the camera pose-based alignment [44], causing misaligned correspondences and inaccurate depth estimates in dynamic objects, which further degrades reconstruction accuracy in static regions. While recent methods such as MonST3R [51] extends training to dynamic-scene video collections to account for dynamic objects, it still models all pointmaps as if generated by a single global rigid transformation. Consequently, these approaches suffer from compromised correspondence learning for dynamic objects, in turn impairing depth accuracy and robust geometry recovery.

In this paper, we propose **D**ynamic **D**ense **U**nconstrained **St**ereo **3**D **R**econstruction (**D^{2}USt3R**), a novel feed-forward framework that directly regresses Static-Dynamic Aligned Pointmaps (SDAP), simultaneously accounting for both spatial structures and temporal motions to enable more reliable 3D reconstruction of both static and dynamic regions. Unlike MonST3R [51], which overlooks correspondences on moving objects, our model captures dense inter-frame matches by treating correspondence and reconstruction as a unified problem in dynamic scenes. We achieve this with a novel training scheme that applies separate supervisory signals to static and dynamic regions, signals that are further stabilized and localized to regions of interests by our occlusion and dynamic masks. Experimental results and visual comparisons confirm that our approach delivers a significant boost in reconstruction accuracy.

Our contributions are summarized as follows:

- Our approach, **D^{2}USt3R**, captures dynamic motion by leveraging static–dynamic aligned pointmaps, allowing for the comprehensive 3D reconstruction of all scene elements in any environment.
- To compensate for the missing direct 3D correspondences between dynamic objects, we propose a 3D alignment loss that effectively accounts for the occlusions and object motions.
- **D^{2}USt3R** achieves state-of-the-art performance across several downstream tasks, including multi-frame depth estimation as well as camera pose estimation, demonstrating superior results in dense 3D reconstruction of dynamic scenes.

2 Related Work

Per-scene 3D reconstruction. Classical 3D reconstruction methods typically follow a multi-stage pipeline to recover scene geometry and camera parameters from a set of uncalibrated images. Prominent examples include Structure-from-Motion (SfM) [52], and Simultaneous Localization and

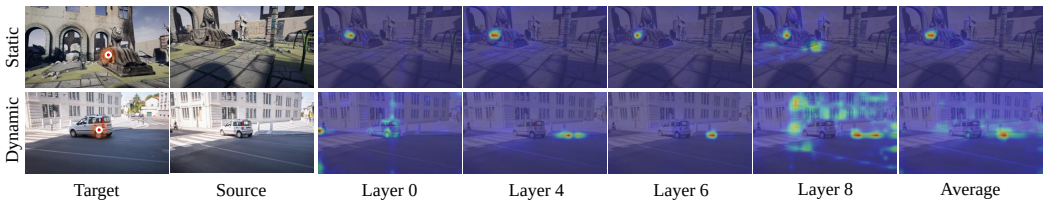

Figure 2: **Cross-attention visualization of DUSt3R [44] on static vs. dynamic scenes.** We show source-image attention maps for a highlighted query point (red) at each layer and averaged across layers. While DUSt3R captures geometric correspondences well in static regions, it fails in dynamic areas due to its rigid-motion, static-frame assumption.

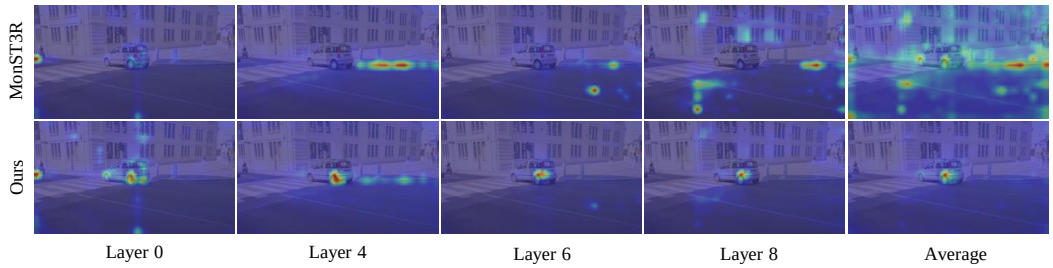

Figure 3: **Cross-attention visualization on dynamic scenes: MonST3R [51] vs. Ours.** Using the same setup as Figure 2, MonST3R inherits DUSt3R's static-scene supervision and fails to align moving regions, limiting reconstruction. In contrast, our method consistently matches dynamic frames and produces sharply localized attention.

Mapping (SLAM) [8]. SfM incrementally reconstructs sparse 3D points through feature matching and bundle adjustment where SLAM simultaneously estimates camera trajectories and builds sparse or semi-dense maps in real-time. Building upon SfM, ParticleSfM [53] incorporate particle-based trajectory modeling to track object motions, paving the way for reconstruction in dynamic scenes. Despite all of these approaches showing remarkable performance, they typically require long processing time and resources for scene-specific optimization and often struggle with error accumulations from multi-stage pipelines.

Learning-based static scene reconstruction. Building on top of estabilished correspondence fields [4, 5, 17, 18, 14], various learning-based approaches [41, 25, 12, 37, 16] have been proposed to reconstruct static 3D scenes by learning strong 3D priors, representing the scene as point clouds [25, 13], meshes [12, 42], voxels [37, 6] and 3DGS [15]. Recently, DUSt3R [44] notably provides a unified, feed-forward pipeline for dense stereo matching, geometry estimation, and triangulation by directly regressing structured 3D pointmaps. Although DUSt3R significantly improves reconstruction quality and efficiency by reducing cumulative errors, DUSt3R is inherently designed for static scenes, limiting its effectiveness in scenarios involving dynamic components.

Learning-based dynamic scene reconstruction. Dynamic scene reconstruction introduces additional complexities due to non-rigid transformations occurring across frames. Similarly to static scene reconstruction, several recent approaches [23, 51, 28, 24, 43, 48] have employed learning-based methods to tackle dynamic scene reconstruction. Among these, MonST3R [51] directly fine-tunes DUSt3R using videos consisting of dynamic scenes. Although it has shown competitive performance, MonST3R retains DUSt3R's per-frame training paradigm and lacks explicit mechanisms for linking corresponding points across frames in dynamic scenes, leading to inconsistent depth estimations that arises from lacking constraints that fail to capture the intricate motion patterns of objects. Our method addresses this limitation by augmenting the existing feed-forward framework with motion-aware training objectives, explicitly enforcing consistent 3D point correspondences over time.

3 Preliminary

Given a pair of input images $I^1, I^2 \in \mathbb{R}^{W\times H\times 3}$, DUSt3R [44] predicts a pair of 3D pointmaps $X^{1,1}, X^{2,1} \in \mathbb{R}^{W\times H\times 3}$ for both images, each expressed in the camera coordinate system of I^1. To train the network in a supervised manner, ground-truth pointmaps for each image are defined in the coordinate space of the first camera. Specifically, given the camera intrinsics matrix $K \in \mathbb{R}^{3\times 3}$,

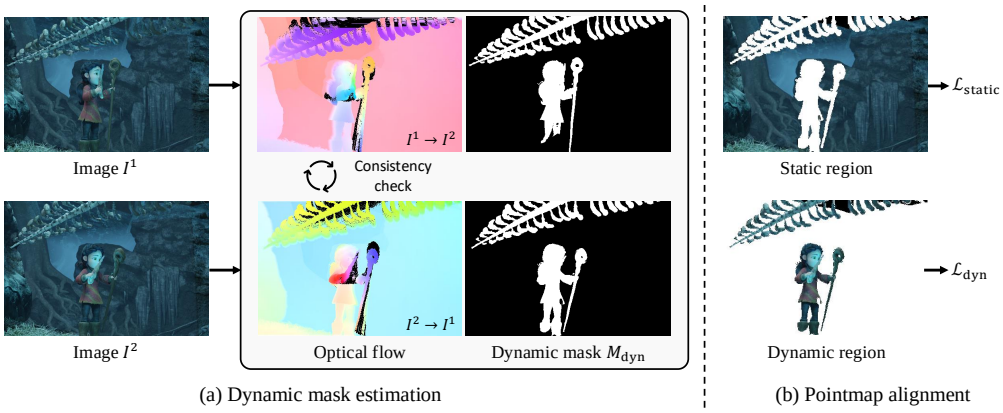

(a) Dynamic mask estimation (b) Pointmap alignment

Figure 4: **Construction of alignment loss defined at static and dynamic regions.** We introduce a pipeline for constructing a static-dynamic aligned pointmap (SDAP) that explicitly handles occlusions in dynamic regions. First, we compute and refine optical flow via cycle consistency checks and derive a dynamic mask M_{dyn}. To align image I^2 with image I^1, we then: 1) warp static pixels using the known camera poses, and 2) warp dynamic pixels using the optical flow. By combining these two warps, we finally obtain SDAP that registers every corresponding 2D pixel into 3D space.

world-to-camera pose matrices $P^n, P^m \in \mathbb{R}^{4\times 4}$ for images n and m, and a ground-truth depth map $D \in \mathbb{R}^{W\times H}$, the ground-truth pointmap is computed as $\bar{X}^{n,m} = P^m(P^n)^{-1}h(K^{-1}D)$, where $h : (x, y, z) \mapsto (x, y, z, 1)$ represents the transformation to homogeneous coordinates.

Using 3D pointmaps, DUSt3R learns its parameters by minimizing the Euclidean distance between the ground-truth pointmaps $\bar{X}^{1,1}$, $\bar{X}^{2,1}$ and the predicted pointmaps $X^{1,1}$, $X^{2,1}$ for two corresponding sets of valid pixels $\mathcal{D}^1, \mathcal{D}^2 \subseteq \{1 \dots W\} \times \{1 \dots H\}$ on which ground-truth defined using a regression loss defined as:

$$\mathcal{L}_{\text{regr}}(v, i) = \left\| \frac{1}{z} X_i^{v,1} - \frac{1}{\bar{z}} \bar{X}_i^{v,1} \right\|, \tag{1}$$

where $v \in \{1, 2\}$ is the input views and $i \in \mathcal{D}^v$ denotes valid pixel positions. The scaling factors $z = \text{norm}(X^{1,1}, X^{2,1})$ and $\bar{z} = \text{norm}(\bar{X}^{1,1}, \bar{X}^{2,1})$ are computed using the normalization function:

$$\text{norm}(X^1, X^2) = \frac{1}{|\mathcal{D}^1| + |\mathcal{D}^2|} \sum_{v\in\{1,2\}} \sum_{i\in\mathcal{D}^v} \|X_i^v\|. \tag{2}$$

Additionally, DUSt3R incorporates a confidence score to learn to reject errorneously defined GT pointmaps, and it is included in the final loss function such that:

$$\mathcal{L}_{\text{conf}} = \sum_{v\in\{1,2\}} \sum_{i\in\mathcal{D}^v} C_i^{v,1} \mathcal{L}_{\text{regr}}(v, i) - \alpha \log C_i^{v,1}. \tag{3}$$

4 Methodology

4.1 Motivation and overview

As shown in Figure 1, DUSt3R [44] predicts 3D pointmaps in static regions with high accuracy, leveraging precise stereo correspondences for robust reconstruction. Inspired by ZeroCo's finding that DUSt3R's cross-attention inherently encodes geometric correspondences [1], we visualize attention maps for both static and dynamic scenes in Figure 2. While DUSt3R excels in static areas, it fails to produce localized attention scores in dynamic regions, leading to noisy pointmap predictions as visualized in Figure 1. To address this, MonST3R [51] augment DUSt3R's training data with dynamic sequences, but they still neglect explicit object-to-object correspondences. This omission prevents dynamic objects from serving as anchors that could strengthen the spatial structure and improve depth estimates of neighboring static regions, thereby limiting overall reconstruction quality. Figure 3 highlights these shortcomings, showing how noisy or missing correspondences degrade accuracy.

To overcome these limitations, we propose Static–Dynamic Aligned Pointmaps (SDAP). Unlike static-only aligned pointmaps, which align 3D points solely with rigid transformations, SDAP

Table 1: **Training datasets.** All datasets consists of synthetic scenes and provide both camera and depth. We excluded scenes containing incomplete dataset annotations or noisy objects (e.g., smoke). Details regarding each scene are documented in the supplementary material.

Dataset	Domain	# of frames	# of Scenes	Dynamics	Dynamic mask	Optical flow	Ratio
Blinkvision Outdoor [22]	Outdoors	6k	23	Realistic	✓	✓	38.75%
Blinkvision Indoor [22]	Indoors	6k	24	Realistic	✓	✓	23.75%
PointOdyssey [54]	Indoors & Outdoors	200k	131	Realistic	✗	✗	12.5%
TartanAir [45]	Indoors & Outdoors	1000k	163	None	✗	✓	12.5%
Spring [29]	Outdoors	6k	37	Realistic	✓	✓	12.5%

simultaneously aligns both static and dynamic components in the scene, fully encoding each pixel's spatial and temporal information. In the following sections, we describe our proposed SDAP representation and outline our training procedure.

4.2 Static-Dynamic Aligned Pointmap

While 3D pointmaps excel at encoding static 3D structure [44], they break down on moving objects due to temporal misalignment. To address this, we introduce Static–Dynamic Aligned Pointmaps (SDAP), which jointly enforce spatial consistency and capture pixel motion across time. Our key insight is to represent every pixel in a unified world coordinate system that aligns its position at each timestep, yielding a cohesive reconstruction of dynamic scenes. However, dynamic motion often leads to occlusions, meaning some pixels appear in only one frame. This results in incomplete alignment, which ultimately limits the quality of 3D reconstruction.

Occlusion Masks. To eliminate occluded regions in our SDAP representation, we first obtain dense 2D correspondences across each image pair using an off-the-shelf optical flow estimator [46]. If ground-truth flows are available in the dataset, we use those instead. In scenarios with large camera baselines, where occlusions become more frequent, we further apply a forward–backward consistency check [39, 50] to derive precise occlusion masks. The full procedure is detailed below.:

$$p_2' = p_1 + \mathbf{f}(p_1), \quad p_1' = p_2' + \mathbf{b}(p_2'), \quad M_{\text{occ}} = [|p_1' - p_1| > t], \tag{4}$$

where p_i denotes a pixel in image I^i, $\mathbf{f}$ and $\mathbf{b}$ represent forward and backward optical flows, respectively, and t is an occlusion threshold.

Dynamic Masks. Dynamic regions, characterized by moving objects and non-rigid transformations, introduce significant challenges in accurately aligning pointmaps due to inconsistencies between camera-induced motion and object-specific motion. Without explicitly accounting for such dynamic behaviors, the network may attempt to incorrectly fit dynamic regions as if they were static, thus impairing reconstruction accuracy. To address this, we introduce a dynamic mask M_{dyn} that explicitly highlights moving regions, guiding the network toward a more stable learning process. Specifically, the dynamic mask M_{dyn} is computed by comparing optical flow $\mathbf{f}$ with the expected flow induced purely by camera motion $\mathbf{f}_{\text{cam}}$. Given the depth map D, intrinsics matrix K, relative rotation and translation R, T, and pixel coordinates p, we define:

$$\mathbf{f}_{\text{cam}} = \pi(DKRK^{-1}p + KT) - p, \quad M_{\text{dyn}} = [\|\mathbf{f}_{\text{cam}} - \mathbf{f}\| > \tau], \tag{5}$$

where $\pi : (x, y, z) \mapsto (x/z, y/z)$ is the projection operation, and τ serves as the dynamic threshold.

4.3 Objective Function

Given our SDAP representation equipped with occlusion and dynamic masks, we formulate our training objective as confidence-aware 3D regression [44], leveraging these masks to achieve enhanced stability. To effectively account for the distinct characteristics of static and dynamic regions, we introduce two separate objective functions, each explicitly designed to handle the respective scenarios and ensure accurate reconstruction in both cases.

Pointmap alignment in static regions. The regression loss in DUSt3R inherently aligns 3D pointmaps using camera pose alone. To ensure alignment focuses solely on static regions within image I^2, we employ the dynamic mask M_{dyn} and restrict the computation of the regression loss

accordingly. Thus, we modify the regression loss $\mathcal{L}_{\text{regr}}$ as follows:

$$\begin{aligned}\mathcal{L}_{\text{regr}}(1,i) &= \left\| \frac{1}{z} X_i^{1,1} - \frac{1}{\bar{z}} \bar{X}_i^{\,1,1} \right\|, \\ \mathcal{L}_{\text{regr}}(2,i) &= \left(1 - M_{\text{dyn},i}^2\right) \left\| \frac{1}{z} X_i^{2,1} - \frac{1}{\bar{z}} \bar{X}_i^{\,2,1} \right\|.\end{aligned} \tag{6}$$

To account for errorneously defined GT pointmaps, we additionally introduce a confidence-aware loss in static regions, $\mathcal{L}_{\text{static}}$, to incorporate uncertainties into the alignment process:

$$\mathcal{L}_{\text{static}} = \sum_{v \in \{1,2\}} \sum_{i \in \mathcal{D}^v} C_i^{v,1} \mathcal{L}_{\text{regr}}(v,i) - \alpha \log C_i^{v,1}. \tag{7}$$

Pointmap alignment in dynamic regions. To align dynamic region from I^2 to I^1, we introduce a dynamic alignment loss that leverages both the occlusion mask M_{occ} and the dynamic mask M_{dyn} to effectively address occlusions and motion. As illustrated in Figure 4, these masks are computed in a dedicated pipeline. This method ensures that when points from the second view I^2, are transformed into the coordinate system of I^1, they accurately correspond to the temporal state of the first view. In line with our regression loss, we further incorporate confidence estimates to define a confidence-aware alignment loss. The dynamic alignment loss is formulated as follows:

$$\begin{aligned}\mathcal{L}_{\text{dyn}} = &\sum_{i \in \mathcal{D}^2} M_{\text{dyn},i}^2 (1 - M_{\text{occ},i}^2) C_i^{2,1} \left\| \frac{1}{\bar{z}_1} \bar{X}_{i+\mathbf{b}(i)}^{1,1} - \frac{1}{z_1} X_i^{2,1} \right\| - \alpha \log C_i^{2,1} \\ &+ \sum_{i \in \mathcal{D}^1} M_{\text{dyn},i}^1 (1 - M_{\text{occ},i}^1) C_i^{1,2} \left\| \frac{1}{\bar{z}_2} \bar{X}_{i+\mathbf{f}(i)}^{2,2} - \frac{1}{z_2} X_i^{1,2} \right\| - \alpha \log C_i^{1,2}.\end{aligned} \tag{8}$$

We leverage optical flow $\mathbf{f}$ to establish dense correspondences between I^1 and I^2, and its reverse direction $\mathbf{b}$. The first term in our loss function enforces the alignment of the pointmap in the coordinate space of the camera system associated with I^1, while the second term introduces a symmetric constraint by aligning the points when the roles of the views are swapped.

Final Objective. Our final objective function is defined as following:

$$\mathcal{L}_{\text{total}} = \mathcal{L}_{\text{static}} + \mathcal{L}_{\text{dyn}}. \tag{9}$$

This combined loss function enables our model to capture precise 3D geometry and robust correspondences in dynamic scenes while retaining DUSt3R's proven benefits in static regions.

4.4 Additional heads for downstream task

To further enhance the capabilities and interpretability of our SDAP framework, we introduce two additional downstream heads dedicated to explicitly modeling dynamic masks and optical flow.

Dynamic mask head. Since our model implicitly encodes regions corresponding to dynamic motion, we explicitly regress dynamic masks using an additional head. Specifically, we predict a single-channel logit map, $\hat{M}_{\text{dyn}}$, using a DPT head [32], structured similarly to our pointmap regression head. We supervise this head using a binary cross-entropy loss defined as follows:

$$\mathcal{L}_{\text{mask}} = -\frac{1}{|\mathcal{D}_{\text{all}}|} \sum_{i \in \mathcal{D}_{\text{all}}} \left[M_{\text{dyn},i} \log(\sigma(\hat{M}_{\text{dyn},i})) + (1 - M_{\text{dyn},i}) \log(1 - \sigma(\hat{M}_{\text{dyn},i})) \right], \tag{10}$$

where $\sigma(\cdot)$ denotes the sigmoid function and $\mathcal{D}_{\text{all}}$ denotes the set of all pixels.

Optical flow head. To accurately estimate optical flow, we incorporate an additional head based on the RAFT architecture [40]. Inspired by recent findings from ZeroCo [1], our flow head utilizes cross-attention maps instead of traditional 4D correlation volumes. The optical flow head is supervised using the Mixture-of-Laplace loss [46].

5 Experiments

5.1 Experimental setup

Implementation details. Building on top of DUSt3R [44], we freeze the encoder and fine-tune only the decoder and the DPT head [32], as done similarly by MonST3R. For each epoch, we

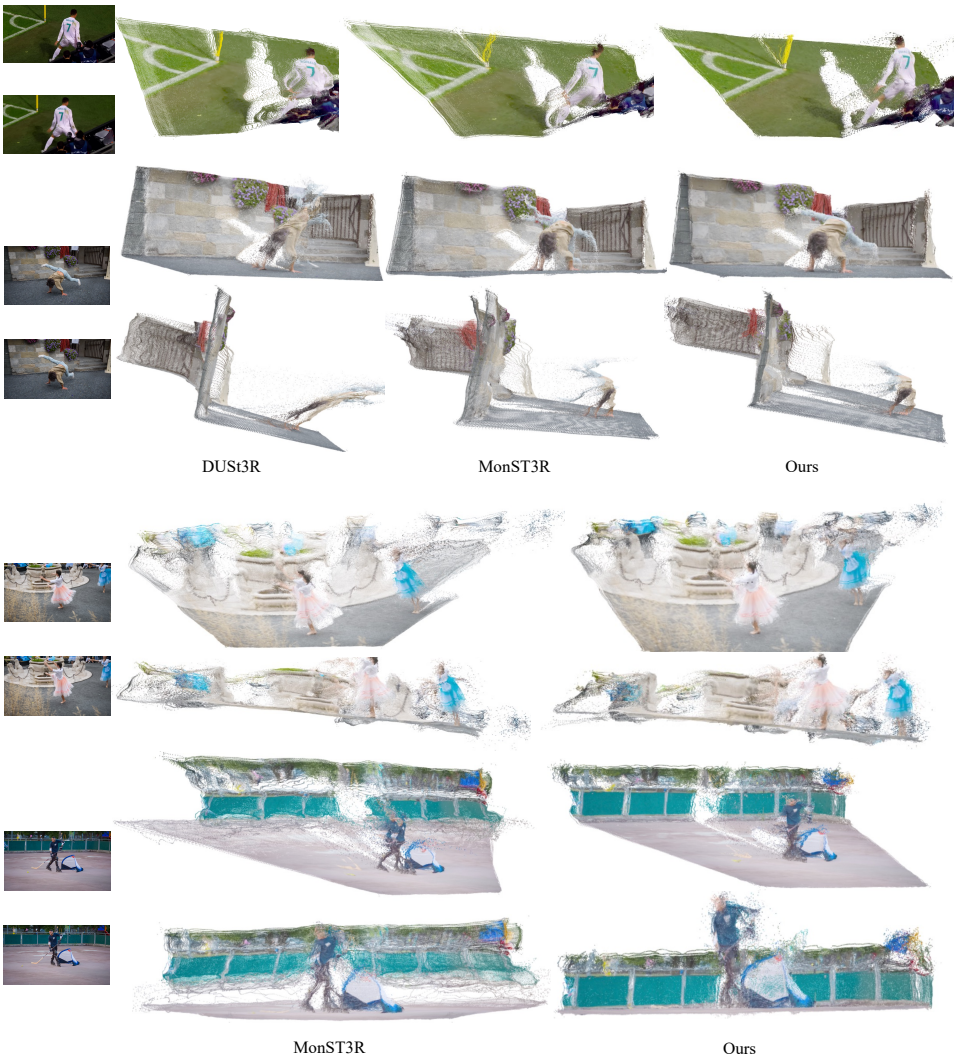

Figure 5: **Pointmap reconstruction.** We qualitatively compare the 3D pointmap of **D^{2}USt3R** against other pointmap regression models [44, 51]. All visualizations presents per-pixel pointmaps without applying confidence thresholding. It is notable that both DUSt3R [44] and MonST3R [51] struggle to accurately reconstruct scenes that include dynamic object. We find that inaccurately established correspondence fields between dynamic regions negatively affect the overall reconstruction performance.

Table 2: **Multi-frame depth estimation results.** We compare multi-frame depth for both the entire scene and dynamic regions separately. The comparison for dynamic regions is conducted only when the dynamic parts are identifiable. *: Reproduced with same dataset as Ours.

Category	Methods	TUM-Dynamics				Bonn				Sintel				KITTI	
		All		Dynamic		All		Dynamic		All		Dynamic		All	
		AbsRel↓	δ_1 ↑	AbsRel↓	δ_1 ↑	AbsRel↓	δ_1 ↑	AbsRel↓	δ_1 ↑	AbsRel↓	δ_1 ↑	AbsRel↓	δ_1 ↑	AbsRel↓	δ_1 ↑
Single-frame depth	DepthAnythingv2 [49]	0.098	89.0	-	-	0.073	93.8	-	-	0.336	55.6	-	-	0.069	93.7
	Marigold [19]	0.205	72.3	-	-	0.066	96.4	-	-	0.623	50.5	-	-	0.104	89.9
Multi-frame depth	DUSt3R [44]	0.176	76.5	0.221	71.3	0.135	82.4	0.127	83.7	0.370	**58.5**	0.672	**54.9**	0.076	93.6
	MASt3R [21]	0.165	79.0	0.199	73.8	0.183	77.5	0.167	79.5	0.330	57.3	0.528	54.4	**0.050**	**96.8**
	MonST3R [51]	0.145	81.2	0.152	79.2	0.068	94.4	0.066	94.9	0.345	56.2	**0.525**	46.9	0.070	95.0
	MonST3R* [51]	0.159	81.0	0.181	76.5	0.076	93.9	0.071	94.4	0.349	52.5	0.565	36.9	0.103	90.9
	D^{2}USt3R (Ours)	**0.142**	**83.9**	**0.148**	**82.9**	**0.060**	**95.8**	**0.059**	**95.7**	**0.324**	57.5	0.568	48.0	0.104	90.7

randomly sample 20,000 image pairs and the network is trained for 50 epochs. We use the AdamW optimizer [27] with an initial learning rate of 5e-5. We train with 4 NVIDIA RTX 6000 GPUs, with a batch size of 4 images per GPU and gradient accumulation steps set to 2.

Training datasets. As shown in Table 1, we train **D^{2}USt3R** on multiple datasets, including BlinkVision Outdoor [22], BlinkVision Indoor [22], Spring [29], PointOdyssey [54], and TartanAir [45]. Each epoch consisted of sampling 7,750, 4,750, 2,500, 2,500, and 2,500 pairs, respectively. Additionally,

Table 3: **Single-frame depth estimation results.** *: Reproduced using the same dataset as ours.

Methods	Bonn		Sintel		KITTI		NYU-v2		TUM-Dynamics	
	AbsRel↓	δ_1 ↑	AbsRel↓	δ_1 ↑	AbsRel↓	δ_1 ↑	AbsRel↓	δ_1 ↑	AbsRel↓	δ_1 ↑
DUSt3R [44]	0.141	82.5	0.424	**58.7**	0.112	86.3	**0.080**	**90.7**	0.176	76.8
MASt3R [21]	0.142	82.0	0.354	57.9	**0.076**	**93.2**	0.129	84.9	0.160	78.7
MonST3R [51]	0.076	93.9	0.345	56.5	0.101	89.3	0.091	88.8	**0.147**	81.1
MonST3R* [51]	0.083	93.6	0.387	50.6	0.143	85.0	0.084	90.1	0.163	79.1
D²USt3R (Ours)	**0.065**	**95.2**	**0.340**	58.4	0.131	86.2	0.085	90.1	0.150	**82.9**

Table 4: **Camera pose estimation results.** *: Reproduced using the same dataset as ours.

Methods	Sintel				TUM-Dynamics				ScanNet			
	Rotation		Translation		Rotation		Translation		Rotation		Translation	
	Avg.↓	Med.↓	Avg.↓	Med.↓	Avg.↓	Med.↓	Avg.↓	Med.↓	Avg.↓	Med.↓	Avg.↓	Med.↓
DUSt3R [44]	6.15	4.51	0.29	0.26	2.36	0.98	0.013	0.01	0.74	0.54	0.11	0.08
MASt3R [21]	4.71	3.40	0.23	0.19	2.83	1.13	0.06	0.03	0.85	0.64	0.05	0.04
MonST3R [51]	4.90	2.30	0.26	0.22	1.88	1.39	0.019	0.01	0.94	0.79	0.10	0.08
MonST3R* [51]	8.50	2.61	0.27	0.23	1.76	1.40	0.02	0.01	0.74	0.58	0.10	0.08
D²USt3R (Ours)	6.96	2.67	0.26	0.22	1.80	1.41	0.03	0.02	0.75	0.57	0.08	0.06

Table 5: **Pointmap alignment accuracy in dynamic objects.** We report End-Point Error (EPE) ↓ on the Sintel and KITTI datasets. Note that Croco-Flow [47] is shown in gray on the Sintel benchmark because it was trained on that dataset. *: Reproduced using the same dataset as ours.

Methods	Sintel-Clean	Sintel-Final	KITTI
DUSt3R [44]	30.96	35.11	14.19
MASt3R [21]	39.37	39.50	13.27
MonST3R [51]	38.47	41.92	14.91
MonST3R* [51]	37.47	40.58	14.58
D²USt3R (Ours)	**16.19**	**25.31**	**8.91**
Croco-Flow [47]	3.31	4.28	13.24
SEA-RAFT [46]	**5.21**	13.18	4.43
D²USt3R + Flow head	9.25	**12.77**	**3.57**

Input image DUSt3R MonST3R Ours

Figure 6: **Depth estimation qualitative results.**

DUSt3R MASt3R MonST3R Ours

Figure 7: **Visualization of correspondences given a pair of images.** We show that our method can find accurate correspondences between dynamic objects.

we perform random sampling with temporal strides varying from 1 to 9 to account for large camera motions and dynamic scenarios.

Baselines. Following [44], we evaluate our method on depth and camera pose estimation. We additionally evaluate pointmap alignment accuracy in dynamic regions. We compare our method against existing state-of-the-art pointmap regression models, specifically DUSt3R [44], MASt3R [21], and MonST3R [51]. Furthermore, to ensure fair comparisons and demonstrate the effectiveness of our approach, we trained a variant of MonST3R, termed MonST3R*, under the same setup as ours.

Evaluation setup. For multi-frame depth estimation, we evaluate on the TUM-Dynamics [38], Bonn [30], Sintel [2], KITTI [11], and ScanNet [7] datasets using image pairs with source frames offset from the target by strides of 1, 3, 5, 7, and 9 frames. We assess performance over the entire scene and exclusively on dynamic regions when dynamic masks are available. For single-

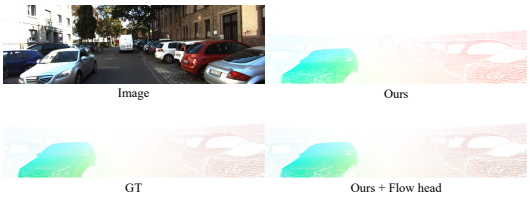

Figure 8: **Predicted optical flow.**

Figure 9: **Predicted dynamic mask.**

Table 6: **Robustness analysis on frame intervals.** We evaluate the robustness of our method with respect to varying frame intervals $\Delta t \in \{1, 3, 5, 7, 9\}$. *: Reproduced using the same dataset as ours.

Methods	$\Delta t = 1$		$\Delta t = 3$		$\Delta t = 5$		$\Delta t = 7$		$\Delta t = 9$	
	AbsRel↓	δ_1 ↑	AbsRel↓	δ_1 ↑	AbsRel↓	δ_1 ↑	AbsRel↓	δ_1 ↑	AbsRel↓	δ_1 ↑
MonST3R*[51]	0.078	93.8	0.078	93.5	0.075	93.9	0.074	93.9	0.072	94.3
D^{2}USt3R (Ours)	0.061	95.6	0.061	95.5	0.060	95.7	0.061	95.9	0.058	96.2

frame depth estimation, we evaluate on the Bonn [30], Sintel [2], KITTI [10], NYU-v2 [36], and TUM-Dynamics [38] datasets. In both settings, we follow the affine-invariant depth evaluation protocol, reporting the Absolute Relative Error (AbsRel) and the percentage of inlier points (δ_1, where $\delta < 1.25$).

5.2 Experimental results

Depth estimation. In this experiment, we evaluate our method and compare with existing methods on single/multi-frame depth estimation. The results are summarized in Table 2 and 3. We also show qualitative comparisons in Figure 5 and Figure 6. From the results, we observe that **D^{2}USt3R** outperforms other methods overall. However, our performance on KITTI is somewhat limited, likely due to the absence of driving scenes in our training data, which may have disadvantaged our model. Nonetheless, we compare with MonST3R*, which was trained with the same training datasets as ours, and find that the performance is comparable. Finally, we highlight in Figure 5 that our approach consistently predicts accurate depth for dynamic human subjects.

Camera pose estimation. In Table 4, we evaluate camera pose performance of our model on the Sintel [2], TUM-dynamics [38] and ScanNet [7] datasets. Note that we use the 2D–3D matching between the prediction $X^{2,1}$ and the original coordinates to obtain camera poses via PNP-RANSAC.

Dynamic alignment. In Table 5, we evaluate pointmap alignment accuracy in dynamic objects. For this, we use Sintel [2] and KITTI [10]. Since we directly obtain aligned pointmaps even in dynamic objects, we can easily derive 2D-2D matching points by computing the difference between $X^{2,1}$ and $X^{1,1}$. From the results, we find that our method outperforms other baselines, which is further supported in Figure 7, where accurately captured correspondences between objects in different time step frames are observed. This gap is further broadened when we leverage an additional flow head, as shown in Table 5, where ours with the flow head outperforms the state-of-the-art SEA-RAFT [46]. We provide qualitative examples in Figure 8.

Dynamic mask. In this experiment, we show that using dynamic mask head, our method reliably predicts dynamic regions. We show visualizations in Figure 9, where the dynamic mask head effectively segments dynamic objects across diverse in-the-wild scenarios.

5.3 Robustness analysis on frame intervals

We evaluate multi-frame depth estimation for the robustness of our method with respect to varying frame intervals on the Bonn dataset [30], as summarized in Table 6. Across all tested intervals ($\Delta t \in \{1, 3, 5, 7, 9\}$), the results show that our model maintains stable performance and even exhibits slight improvement as the interval widens, demonstrating strong temporal consistency and resilience to larger motion baselines. These results suggest that the proposed flow-chaining strategy effectively preserves geometric coherence across diverse motion dynamics, enabling reliable depth estimation under varying temporal conditions.

5.4 Ablation study

Table 7: **Ablation on training strategy.**

Methods	TUM-Dynamics		Bonn	
	AbsRel↓	δ_1 ↑	AbsRel↓	δ_1 ↑
Full finetune	0.161	77.0	0.081	91.9
Finetune decoder & head	0.142	83.9	0.060	95.8

Although we've already validated our 3D alignment loss and effectiveness of proposed SDAP, we further examine how different fine-tuning strategies affect performance. Since our method, unlike DUSt3R or MonST3R, learns precise maps of cross-attention (Figure 3), we ask whether updating the encoder along with the decoder and head yields gains. As shown in Table 7, fine-tuning only the decoder and downstream head actually outperforms full fine-tuning. Therefore, in this work we restrict training to the decoder and head.

6 Conclusion

In this paper, we have introduced a novel approach for 3D dynamic scene reconstruction, featuring a simple yet effective extension to existing pointmap representations to accommodate dynamic motions. Our proposed method significantly enhances the quality of 3D reconstruction in dynamic environments. We evaluated our approach comprehensively across tasks including depth estimation, camera pose estimation, and 3D point alignment. Experimental results demonstrate that our method outperforms existing approaches on real-world, large-scale datasets, achieving new state-of-the-art performance.

Acknowledgments and Disclosure of Funding

This research was supported by Institute of Information & communications Technology Planning & Evaluation (IITP) grant funded by the Korea government (MSIT) (RS-2019-II190075, RS-2024-00509279, RS-2025-II212068, RS-2023-00227592, RS-2025-02214479, RS-2024-00457882, RS-2025-25441838, RS-2025-25441838, RS-2025-02214479, RS-2025-02217259) and the Culture, Sports, and Tourism R&D Program through the Korea Creative Content Agency grant funded by the Ministry of Culture, Sports and Tourism (RS-2024-00345025, RS-2024-00333068, RS-2023-00222280, RS-2023-00266509), and National Research Foundation of Korea (RS-2024-00346597).

This research was supported by the ETH AI Center through an ETH AI Center postdoctoral fellowship to Sunghwan Hong.

References

[1] Honggyu An, Jinhyeon Kim, Seonghoon Park, Jaewoo Jung, Jisang Han, Sunghwan Hong, and Seungryong Kim. Cross-view completion models are zero-shot correspondence estimators. *arXiv preprint arXiv:2412.09072*, 2024.

[2] Daniel J Butler, Jonas Wulff, Garrett B Stanley, and Michael J Black. A naturalistic open source movie for optical flow evaluation. In *Computer Vision–ECCV 2012: 12th European Conference on Computer Vision, Florence, Italy, October 7-13, 2012, Proceedings, Part VI 12*, pages 611–625. Springer, 2012.

[3] Carlos Campos, Richard Elvira, Juan J Gómez Rodríguez, José MM Montiel, and Juan D Tardós. Orb-slam3: An accurate open-source library for visual, visual–inertial, and multimap slam. *IEEE Transactions on Robotics*, 37(6):1874–1890, 2021.

[4] Seokju Cho, Sunghwan Hong, Sangryul Jeon, Yunsung Lee, Kwanghoon Sohn, and Seungryong Kim. Cats: Cost aggregation transformers for visual correspondence. *Advances in Neural Information Processing Systems*, 34:9011–9023, 2021.

[5] Seokju Cho, Sunghwan Hong, and Seungryong Kim. Cats++: Boosting cost aggregation with convolutions and transformers. *IEEE Transactions on Pattern Analysis and Machine Intelligence*, 45(6):7174–7194, 2022.

[6] Christopher B Choy, Danfei Xu, JunYoung Gwak, Kevin Chen, and Silvio Savarese. 3d-r2n2: A unified approach for single and multi-view 3d object reconstruction. In *Computer Vision–ECCV 2016: 14th European Conference, Amsterdam, The Netherlands, October 11-14, 2016, Proceedings, Part VIII 14*, pages 628–644. Springer, 2016.

[7] Angela Dai, Angel X Chang, Manolis Savva, Maciej Halber, Thomas Funkhouser, and Matthias Nießner. Scannet: Richly-annotated 3d reconstructions of indoor scenes. In *Proceedings of the IEEE conference on computer vision and pattern recognition*, pages 5828–5839, 2017.

[8] Andrew J Davison, Ian D Reid, Nicholas D Molton, and Olivier Stasse. Monoslam: Real-time single camera slam. *IEEE transactions on pattern analysis and machine intelligence*, 29(6):1052–1067, 2007.

[9] Yasutaka Furukawa, Carlos Hernández, et al. Multi-view stereo: A tutorial. *Foundations and Trends® in Computer Graphics and Vision*, 9(1-2):1–148, 2015.

[10] Andreas Geiger, Martin Lauer, Christian Wojek, Christoph Stiller, and Raquel Urtasun. 3d traffic scene understanding from movable platforms. *IEEE transactions on pattern analysis and machine intelligence*, 36(5):1012–1025, 2013.

[11] Andreas Geiger, Philip Lenz, Christoph Stiller, and Raquel Urtasun. Vision meets robotics: The kitti dataset. *The international journal of robotics research*, 32(11):1231–1237, 2013.

[12] Georgia Gkioxari, Jitendra Malik, and Justin Johnson. Mesh r-cnn. In *Proceedings of the IEEE/CVF international conference on computer vision*, pages 9785–9795, 2019.

[13] Yulan Guo, Hanyun Wang, Qingyong Hu, Hao Liu, Li Liu, and Mohammed Bennamoun. Deep learning for 3d point clouds: A survey. *IEEE transactions on pattern analysis and machine intelligence*, 43(12):4338–4364, 2020.

[14] Sunghwan Hong, Seokju Cho, Jisu Nam, Stephen Lin, and Seungryong Kim. Cost aggregation with 4d convolutional swin transformer for few-shot segmentation. In *European Conference on Computer Vision*, pages 108–126. Springer, 2022.

[15] Sunghwan Hong, Jaewoo Jung, Heeseong Shin, Jisang Han, Jiaolong Yang, Chong Luo, and Seungryong Kim. Pf3plat: Pose-free feed-forward 3d gaussian splatting. *arXiv preprint arXiv:2410.22128*, 2024.

[16] Sunghwan Hong, Jaewoo Jung, Heeseong Shin, Jiaolong Yang, Seungryong Kim, and Chong Luo. Unifying correspondence pose and nerf for generalized pose-free novel view synthesis. In *Proceedings of the IEEE/CVF Conference on Computer Vision and Pattern Recognition*, pages 20196–20206, 2024.

[17] Sunghwan Hong and Seungryong Kim. Deep matching prior: Test-time optimization for dense correspondence. In *Proceedings of the IEEE/CVF international conference on computer vision*, pages 9907–9917, 2021.

[18] Sunghwan Hong, Jisu Nam, Seokju Cho, Susung Hong, Sangryul Jeon, Dongbo Min, and Seungryong Kim. Neural matching fields: Implicit representation of matching fields for visual correspondence. *Advances in Neural Information Processing Systems*, 35:13512–13526, 2022.

[19] Bingxin Ke, Anton Obukhov, Shengyu Huang, Nando Metzger, Rodrigo Caye Daudt, and Konrad Schindler. Repurposing diffusion-based image generators for monocular depth estimation. In *Proceedings of the IEEE/CVF Conference on Computer Vision and Pattern Recognition (CVPR)*, 2024.

[20] Bernhard Kerbl, Georgios Kopanas, Thomas Leimkühler, and George Drettakis. 3d gaussian splatting for real-time radiance field rendering. *ACM Trans. Graph.*, 42(4):139–1, 2023.

[21] Vincent Leroy, Yohann Cabon, and Jérôme Revaud. Grounding image matching in 3d with mast3r. *arXiv preprint arXiv:2406.09756*, 2024.

[22] Yijin Li, Yichen Shen, Zhaoyang Huang, Shuo Chen, Weikang Bian, Xiaoyu Shi, Fu-Yun Wang, Keqiang Sun, Hujun Bao, Zhaopeng Cui, et al. Blinkvision: A benchmark for optical flow, scene flow and point tracking estimation using rgb frames and events. In *European Conference on Computer Vision*, pages 19–36. Springer, 2024.

[23] Zhengqi Li, Richard Tucker, Forrester Cole, Qianqian Wang, Linyi Jin, Vickie Ye, Angjoo Kanazawa, Aleksander Holynski, and Noah Snavely. Megasam: Accurate, fast, and robust structure and motion from casual dynamic videos. *arXiv preprint arXiv:2412.04463*, 2024.

[24] Yiqing Liang, Abhishek Badki, Hang Su, James Tompkin, and Orazio Gallo. Zero-shot monocular scene flow estimation in the wild. *arXiv preprint arXiv:2501.10357*, 2025.

[25] Chen-Hsuan Lin, Chen Kong, and Simon Lucey. Learning efficient point cloud generation for dense 3d object reconstruction. In *proceedings of the AAAI Conference on Artificial Intelligence*, volume 32, 2018.

[26] Philipp Lindenberger, Paul-Edouard Sarlin, Viktor Larsson, and Marc Pollefeys. Pixel-perfect structure-from-motion with featuremetric refinement. In *Proceedings of the IEEE/CVF international conference on computer vision*, pages 5987–5997, 2021.

[27] Ilya Loshchilov and Frank Hutter. Decoupled weight decay regularization. *arXiv preprint arXiv:1711.05101*, 2017.

[28] Jiahao Lu, Tianyu Huang, Peng Li, Zhiyang Dou, Cheng Lin, Zhiming Cui, Zhen Dong, Sai-Kit Yeung, Wenping Wang, and Yuan Liu. Align3r: Aligned monocular depth estimation for dynamic videos. *arXiv preprint arXiv:2412.03079*, 2024.

[29] Lukas Mehl, Jenny Schmalfuss, Azin Jahedi, Yaroslava Nalivayko, and Andrés Bruhn. Spring: A high-resolution high-detail dataset and benchmark for scene flow, optical flow and stereo. In *Proceedings of the IEEE/CVF Conference on Computer Vision and Pattern Recognition*, pages 4981–4991, 2023.

[30] Emanuele Palazzolo, Jens Behley, Philipp Lottes, Philippe Giguere, and Cyrill Stachniss. Refusion: 3d reconstruction in dynamic environments for rgb-d cameras exploiting residuals. In *2019 IEEE/RSJ International Conference on Intelligent Robots and Systems (IROS)*, pages 7855–7862. IEEE, 2019.

[31] Jordi Pont-Tuset, Federico Perazzi, Sergi Caelles, Pablo Arbeláez, Alex Sorkine-Hornung, and Luc Van Gool. The 2017 davis challenge on video object segmentation. *arXiv preprint arXiv:1704.00675*, 2017.

[32] René Ranftl, Alexey Bochkovskiy, and Vladlen Koltun. Vision transformers for dense prediction. In *Proceedings of the IEEE/CVF international conference on computer vision*, pages 12179–12188, 2021.

[33] Johannes L Schonberger and Jan-Michael Frahm. Structure-from-motion revisited. In *Proceedings of the IEEE conference on computer vision and pattern recognition*, pages 4104–4113, 2016.

[34] Thomas Schops, Johannes L Schonberger, Silvano Galliani, Torsten Sattler, Konrad Schindler, Marc Pollefeys, and Andreas Geiger. A multi-view stereo benchmark with high-resolution images and multi-camera videos. In *Proceedings of the IEEE conference on computer vision and pattern recognition*, pages 3260–3269, 2017.

[35] Steven M Seitz, Brian Curless, James Diebel, Daniel Scharstein, and Richard Szeliski. A comparison and evaluation of multi-view stereo reconstruction algorithms. In *2006 IEEE computer society conference on computer vision and pattern recognition (CVPR'06)*, volume 1, pages 519–528. IEEE, 2006.

[36] Nathan Silberman, Derek Hoiem, Pushmeet Kohli, and Rob Fergus. Indoor segmentation and support inference from rgbd images. In *Computer Vision–ECCV 2012: 12th European Conference on Computer Vision, Florence, Italy, October 7-13, 2012, Proceedings, Part V 12*, pages 746–760. Springer, 2012.

[37] Vincent Sitzmann, Justus Thies, Felix Heide, Matthias Nießner, Gordon Wetzstein, and Michael Zollhofer. Deepvoxels: Learning persistent 3d feature embeddings. In *Proceedings of the IEEE/CVF Conference on Computer Vision and Pattern Recognition*, pages 2437–2446, 2019.

[38] Jürgen Sturm, Nikolas Engelhard, Felix Endres, Wolfram Burgard, and Daniel Cremers. A benchmark for the evaluation of rgb-d slam systems. In *2012 IEEE/RSJ international conference on intelligent robots and systems*, pages 573–580. IEEE, 2012.

[39] Narayanan Sundaram, Thomas Brox, and Kurt Keutzer. Dense point trajectories by gpu-accelerated large displacement optical flow. In *European conference on computer vision*, pages 438–451. Springer, 2010.

[40] Zachary Teed and Jia Deng. Raft: Recurrent all-pairs field transforms for optical flow. In *Computer Vision–ECCV 2020: 16th European Conference, Glasgow, UK, August 23–28, 2020, Proceedings, Part II 16*, pages 402–419. Springer, 2020.

[41] Jianyuan Wang, Nikita Karaev, Christian Rupprecht, and David Novotny. Vggsfm: Visual geometry grounded deep structure from motion. In *Proceedings of the IEEE/CVF conference on computer vision and pattern recognition*, pages 21686–21697, 2024.

[42] Nanyang Wang, Yinda Zhang, Zhuwen Li, Yanwei Fu, Wei Liu, and Yu-Gang Jiang. Pixel2mesh: Generating 3d mesh models from single rgb images. In *Proceedings of the European conference on computer vision (ECCV)*, pages 52–67, 2018.

[43] Qianqian Wang, Yifei Zhang, Aleksander Holynski, Alexei A Efros, and Angjoo Kanazawa. Continuous 3d perception model with persistent state. *arXiv preprint arXiv:2501.12387*, 2025.

[44] Shuzhe Wang, Vincent Leroy, Yohann Cabon, Boris Chidlovskii, and Jerome Revaud. Dust3r: Geometric 3d vision made easy. In *Proceedings of the IEEE/CVF Conference on Computer Vision and Pattern Recognition*, pages 20697–20709, 2024.

[45] Wenshan Wang, Delong Zhu, Xiangwei Wang, Yaoyu Hu, Yuheng Qiu, Chen Wang, Yafei Hu, Ashish Kapoor, and Sebastian Scherer. Tartanair: A dataset to push the limits of visual slam. In *2020 IEEE/RSJ International Conference on Intelligent Robots and Systems (IROS)*, pages 4909–4916. IEEE, 2020.

[46] Yihan Wang, Lahav Lipson, and Jia Deng. Sea-raft: Simple, efficient, accurate raft for optical flow. In *European Conference on Computer Vision*, pages 36–54. Springer, 2024.

[47] Philippe Weinzaepfel, Thomas Lucas, Vincent Leroy, Yohann Cabon, Vaibhav Arora, Romain Brégier, Gabriela Csurka, Leonid Antsfeld, Boris Chidlovskii, and Jérôme Revaud. Croco v2: Improved cross-view completion pre-training for stereo matching and optical flow. In *Proceedings of the IEEE/CVF International Conference on Computer Vision*, pages 17969–17980, 2023.

[48] Jianing Yang, Alexander Sax, Kevin J Liang, Mikael Henaff, Hao Tang, Ang Cao, Joyce Chai, Franziska Meier, and Matt Feiszli. Fast3r: Towards 3d reconstruction of 1000+ images in one forward pass. *arXiv preprint arXiv:2501.13928*, 2025.

[49] Lihe Yang, Bingyi Kang, Zilong Huang, Zhen Zhao, Xiaogang Xu, Jiashi Feng, and Hengshuang Zhao. Depth anything v2. *arXiv:2406.09414*, 2024.

[50] Zhichao Yin and Jianping Shi. Geonet: Unsupervised learning of dense depth, optical flow and camera pose. In *Proceedings of the IEEE conference on computer vision and pattern recognition*, pages 1983–1992, 2018.

[51] Junyi Zhang, Charles Herrmann, Junhwa Hur, Varun Jampani, Trevor Darrell, Forrester Cole, Deqing Sun, and Ming-Hsuan Yang. Monst3r: A simple approach for estimating geometry in the presence of motion. *arXiv preprint arXiv:2410.03825*, 2024.

[52] Zhoutong Zhang, Forrester Cole, Zhengqi Li, Michael Rubinstein, Noah Snavely, and William T Freeman. Structure and motion from casual videos. In *European Conference on Computer Vision*, pages 20–37. Springer, 2022.

[53] Wang Zhao, Shaohui Liu, Hengkai Guo, Wenping Wang, and Yong-Jin Liu. Particlesfm: Exploiting dense point trajectories for localizing moving cameras in the wild. In *European Conference on Computer Vision*, pages 523–542. Springer, 2022.

[54] Yang Zheng, Adam W Harley, Bokui Shen, Gordon Wetzstein, and Leonidas J Guibas. Pointodyssey: A large-scale synthetic dataset for long-term point tracking. In *Proceedings of the IEEE/CVF International Conference on Computer Vision*, pages 19855–19865, 2023.

Enhancing 3D Reconstruction for Dynamic Scenes

- Supplementary Materials -

Jisang Han[1*] **Honggyu An**[1*] **Jaewoo Jung**[1*] **Takuya Narihira**[2] **Junyoung Seo**[1]
Kazumi Fukuda[2] **Chaehyun Kim**[1] **Sunghwan Hong**[3] **Yuki Mitsufuji**[2,4†] **Seungryong Kim**[1†]

[1] KAIST AI [2] Sony AI [3] ETH Zürich AI Center, CVG, PRS [4] Sony Group Corporation

https://cvlab-kaist.github.io/DDUSt3R

A. Training dataset

Table 8: **List of excluded scenes from the datasets.**

Dataset	Excluded Scenes
PointOdyssey	animal_s, animal_smoke_, animal1_s_, animal1_s, animal2_s, animal3_s, animal4_s, animal6_s, cab_e_ego2, cab_e1_3rd, cab_e1_ego2, cab_h_bench_3rd, cab_h_bench_ego2, character0_f, character0_f2, character3_f, character4_, character5_, character6, cnb_dlab_0215_3rd, cnb_dlab_0215_ego1, cnb_dlab_0225_3rd, cnb_dlab_0225_ego1, dancingroom_3rd, human_in_scene, kg, r5_new_f, scene_d78_0318_3rd, scene_d78_0318_ego1, scene_d78_0318_ego2, scene_j716_3rd, scene_j716_ego1, scene_j716_ego2, scene1_0129, seminar_h52_ego1
Blinkvision Outdoor	outdoor_train_autopilot_tree_01, outdoor_train_autopilot_tree_02, outdoor_train_autopilot_tree_03, outdoor_train_track_animal_people

We provide the scene names that were excluded during our training. These scenes are excluded, either because their annotations include errors. Please refer to Table 8.

B. Bullet time reconstruction for dynamic video input

Owing to dynamic alignment and SDAP, we can aggregate and render a highly dynamic video input into a single, coherent bullet-time view. As illustrated in Figure 10, a video consisting of large input frames can be aligned into an intermediate bullet-time representation. This approach enables static reconstruction even when the input video includes dynamic motion. Consequently, it becomes feasible to directly train a 3D Gaussian splatting [20] on scenes containing moving people in landmarks or dynamics that are challenging to render using conventional methods.

39th Conference on Neural Information Processing Systems (NeurIPS 2025).

Input video

Ours

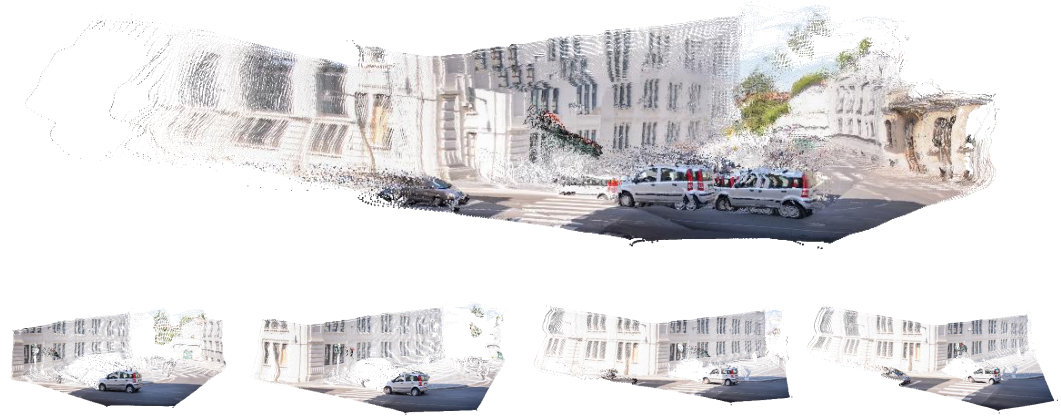

MonST3R

Figure 10: **Visualization of bullet-time reconstruction from a long sequence of dynamic video inputs.** We visualize the reconstruction of bullet-time view (20 frames) from a dynamic video input consisting of 40 frames. Since MonST3R is incapable of dynamic alignment, it predicts depth independently at each timestep, similar to monocular depth estimation, resulting in the reconstruction as a sequence of 3D pointmaps.

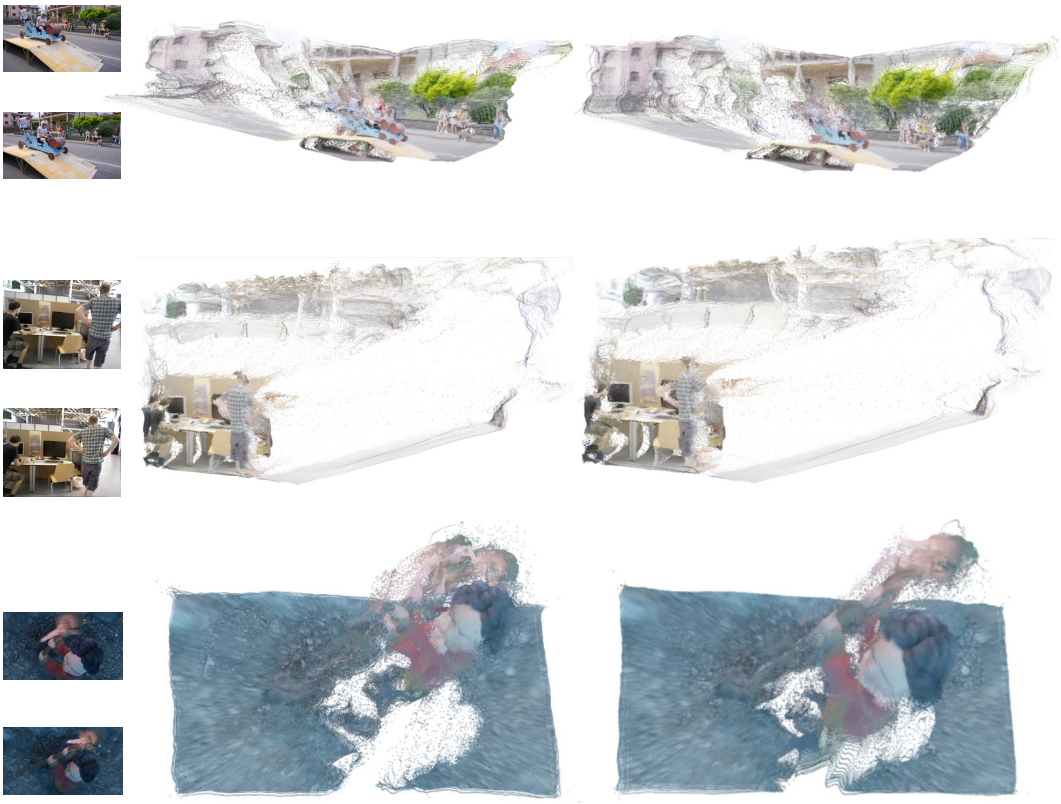

MonST3R Ours

Figure 11: **Additional qualitative results for pointmap reconstruction.** We qualitatively compare the 3D pointmap of **D^{2}USt3R** against MonST3R. All visualizations presents per-pixel pointmaps without applying confidence thresholding.

Input image DUSt3R MonST3R Ours

Figure 12: **Additional qualitative results for depth estimation on Sintel dataset.**

C. Additional results

In Figure 11 and Figure 12, we additionally present qualitative results for pointmap reconstruction and depth estimation. Utilizing our SDAP, dynamic elements are well-aligned, thereby enhancing both depth estimation and 3D reconstruction quality. In Figure 13 and Figure 14, we present qualitative results for optical flow on DAVIS [31] and KITTI [11] datasets. We observed that **D^{2}USt3R** is capable of accurately predicting optical flow without relying on any dedicated optical flow module.

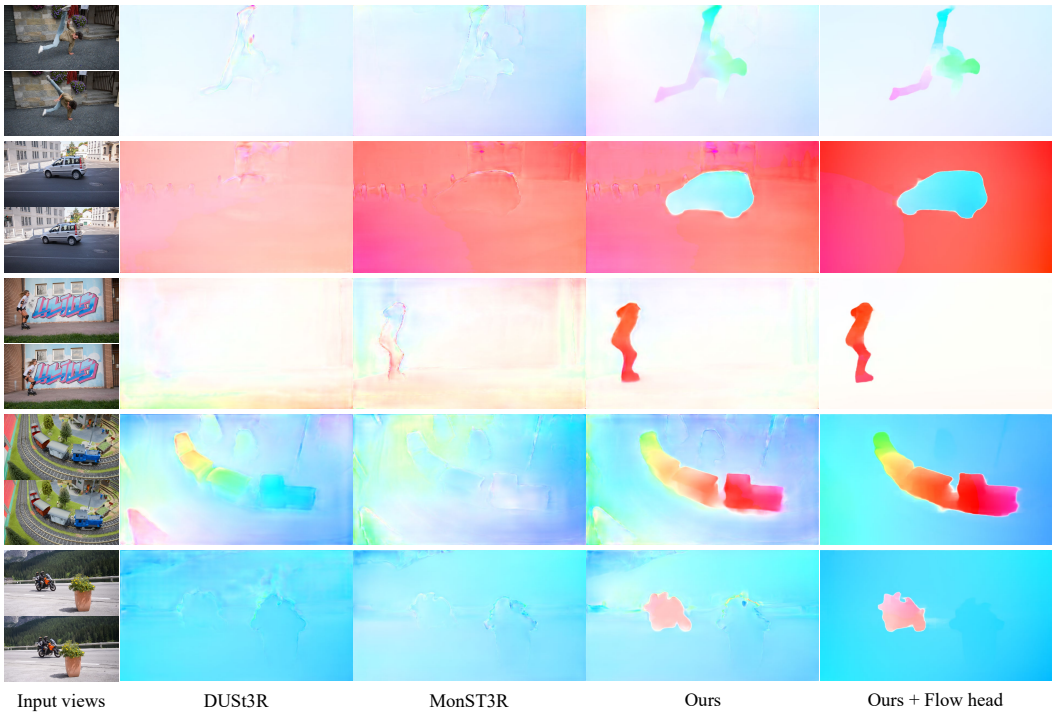

Figure 13: **Qualitative results for optical flow estimation on DAVIS dataset.**

Figure 14: **Qualitative results for optical flow estimation on KITTI dataset.**

Table 9: **Multi-frame depth estimation results on end-to-end integration analysis.**

Methods	TUM-Dynamics		Bonn		Sintel		KITTI	
	AbsRel↓	δ_1 ↑	AbsRel↓	δ_1 ↑	AbsRel↓	δ_1 ↑	AbsRel↓	δ_1 ↑
D^{2}USt3R	0.142	83.9	0.060	95.8	0.324	57.5	0.104	90.7
D^{2}USt3R + Dynamic mask head	0.140	84.4	0.059	95.6	0.313	58.3	0.105	90.3

D. End-to-end dynamic mask head integration

We further explored an end-to-end training strategy in which the entire network, including the dynamic mask head, is jointly optimized. As shown in Table 9, this integrated setup encourages implicit interactions between sub-tasks through shared representations, leading to consistent, albeit moderate, performance improvements. Specifically, we observe gains on two of the four benchmarks, with a mean reduction in AbsRel of 1.7% and a mean increase in δ of 0.9 percentage points. These results confirm that joint optimization promotes beneficial cross-task interactions, yielding complementary improvements across depth and dynamic mask estimation.

E. Limitations

Despite effectively handling dynamic scenarios, our dynamic alignment process has certain limitations. Since our model relies on an off-the-shelf optical flow model, its performance is dependent on the quality of the predicted optical flow. Additionally, our model is non-generative and can only take two frames as input. Because we aim to achieve alignment across time, extending our approach to video input would require an additional global optimization technique.

NeurIPS Paper Checklist

1. **Claims**

   Question: Do the main claims made in the abstract and introduction accurately reflect the paper's contributions and scope?

   Answer: [Yes]

   Justification: In the abstract and introduction (Section 1), we clearly state the assumptions, claims, and contributions of this paper. Furthermore, the analysis (Section 4.1) and experimental evidence (Section 5) are consistent with these claims.

   Guidelines:

   - The answer NA means that the abstract and introduction do not include the claims made in the paper.
   - The abstract and/or introduction should clearly state the claims made, including the contributions made in the paper and important assumptions and limitations. A No or NA answer to this question will not be perceived well by the reviewers.
   - The claims made should match theoretical and experimental results, and reflect how much the results can be expected to generalize to other settings.
   - It is fine to include aspirational goals as motivation as long as it is clear that these goals are not attained by the paper.

2. **Limitations**

   Question: Does the paper discuss the limitations of the work performed by the authors?

   Answer: [Yes]

   Justification: In Section D, we discuss the limitations of our approach.

   Guidelines:

   - The answer NA means that the paper has no limitation while the answer No means that the paper has limitations, but those are not discussed in the paper.
   - The authors are encouraged to create a separate "Limitations" section in their paper.
   - The paper should point out any strong assumptions and how robust the results are to violations of these assumptions (e.g., independence assumptions, noiseless settings, model well-specification, asymptotic approximations only holding locally). The authors should reflect on how these assumptions might be violated in practice and what the implications would be.
   - The authors should reflect on the scope of the claims made, e.g., if the approach was only tested on a few datasets or with a few runs. In general, empirical results often depend on implicit assumptions, which should be articulated.
   - The authors should reflect on the factors that influence the performance of the approach. For example, a facial recognition algorithm may perform poorly when image resolution is low or images are taken in low lighting. Or a speech-to-text system might not be used reliably to provide closed captions for online lectures because it fails to handle technical jargon.
   - The authors should discuss the computational efficiency of the proposed algorithms and how they scale with dataset size.
   - If applicable, the authors should discuss possible limitations of their approach to address problems of privacy and fairness.
   - While the authors might fear that complete honesty about limitations might be used by reviewers as grounds for rejection, a worse outcome might be that reviewers discover limitations that aren't acknowledged in the paper. The authors should use their best judgment and recognize that individual actions in favor of transparency play an important role in developing norms that preserve the integrity of the community. Reviewers will be specifically instructed to not penalize honesty concerning limitations.

3. **Theory assumptions and proofs**

   Question: For each theoretical result, does the paper provide the full set of assumptions and a complete (and correct) proof?

Answer: [NA]

Justification: Our paper does not include theoretical results.

Guidelines:

- The answer NA means that the paper does not include theoretical results.
- All the theorems, formulas, and proofs in the paper should be numbered and cross-referenced.
- All assumptions should be clearly stated or referenced in the statement of any theorems.
- The proofs can either appear in the main paper or the supplemental material, but if they appear in the supplemental material, the authors are encouraged to provide a short proof sketch to provide intuition.
- Inversely, any informal proof provided in the core of the paper should be complemented by formal proofs provided in appendix or supplemental material.
- Theorems and Lemmas that the proof relies upon should be properly referenced.

4. **Experimental result reproducibility**

   Question: Does the paper fully disclose all the information needed to reproduce the main experimental results of the paper to the extent that it affects the main claims and/or conclusions of the paper (regardless of whether the code and data are provided or not)?

   Answer: [Yes]

   Justification: We describe the dataset construction in Sections 4.2, the implementation of the loss functions in Section 4.3 and 4.4, and the implementation details in Section 5.1.

   Guidelines:

   - The answer NA means that the paper does not include experiments.
   - If the paper includes experiments, a No answer to this question will not be perceived well by the reviewers: Making the paper reproducible is important, regardless of whether the code and data are provided or not.
   - If the contribution is a dataset and/or model, the authors should describe the steps taken to make their results reproducible or verifiable.
   - Depending on the contribution, reproducibility can be accomplished in various ways. For example, if the contribution is a novel architecture, describing the architecture fully might suffice, or if the contribution is a specific model and empirical evaluation, it may be necessary to either make it possible for others to replicate the model with the same dataset, or provide access to the model. In general. releasing code and data is often one good way to accomplish this, but reproducibility can also be provided via detailed instructions for how to replicate the results, access to a hosted model (e.g., in the case of a large language model), releasing of a model checkpoint, or other means that are appropriate to the research performed.
   - While NeurIPS does not require releasing code, the conference does require all submissions to provide some reasonable avenue for reproducibility, which may depend on the nature of the contribution. For example
     (a) If the contribution is primarily a new algorithm, the paper should make it clear how to reproduce that algorithm.
     (b) If the contribution is primarily a new model architecture, the paper should describe the architecture clearly and fully.
     (c) If the contribution is a new model (e.g., a large language model), then there should either be a way to access this model for reproducing the results or a way to reproduce the model (e.g., with an open-source dataset or instructions for how to construct the dataset).
     (d) We recognize that reproducibility may be tricky in some cases, in which case authors are welcome to describe the particular way they provide for reproducibility. In the case of closed-source models, it may be that access to the model is limited in some way (e.g., to registered users), but it should be possible for other researchers to have some path to reproducing or verifying the results.

5. **Open access to data and code**

Question: Does the paper provide open access to the data and code, with sufficient instructions to faithfully reproduce the main experimental results, as described in supplemental material?

Answer: [No]

Justification: Due to the large size of the pretrained weights, we plan to release them publicly at a later time.

Guidelines:

- The answer NA means that paper does not include experiments requiring code.
- Please see the NeurIPS code and data submission guidelines (`https://nips.cc/public/guides/CodeSubmissionPolicy`) for more details.
- While we encourage the release of code and data, we understand that this might not be possible, so "No" is an acceptable answer. Papers cannot be rejected simply for not including code, unless this is central to the contribution (e.g., for a new open-source benchmark).
- The instructions should contain the exact command and environment needed to run to reproduce the results. See the NeurIPS code and data submission guidelines (`https://nips.cc/public/guides/CodeSubmissionPolicy`) for more details.
- The authors should provide instructions on data access and preparation, including how to access the raw data, preprocessed data, intermediate data, and generated data, etc.
- The authors should provide scripts to reproduce all experimental results for the new proposed method and baselines. If only a subset of experiments are reproducible, they should state which ones are omitted from the script and why.
- At submission time, to preserve anonymity, the authors should release anonymized versions (if applicable).
- Providing as much information as possible in supplemental material (appended to the paper) is recommended, but including URLs to data and code is permitted.

6. **Experimental setting/details**

Question: Does the paper specify all the training and test details (e.g., data splits, hyperparameters, how they were chosen, type of optimizer, etc.) necessary to understand the results?

Answer: [Yes]

Justification: We provide all training and testing details necessary to understand the results in Section 5.1.

Guidelines:

- The answer NA means that the paper does not include experiments.
- The experimental setting should be presented in the core of the paper to a level of detail that is necessary to appreciate the results and make sense of them.
- The full details can be provided either with the code, in appendix, or as supplemental material.

7. **Experiment statistical significance**

Question: Does the paper report error bars suitably and correctly defined or other appropriate information about the statistical significance of the experiments?

Answer: [No]

Justification: Since our model does not involve any randomness during inference when trained weights are used, we do not report error bars.

Guidelines:

- The answer NA means that the paper does not include experiments.
- The authors should answer "Yes" if the results are accompanied by error bars, confidence intervals, or statistical significance tests, at least for the experiments that support the main claims of the paper.

- The factors of variability that the error bars are capturing should be clearly stated (for example, train/test split, initialization, random drawing of some parameter, or overall run with given experimental conditions).
- The method for calculating the error bars should be explained (closed form formula, call to a library function, bootstrap, etc.)
- The assumptions made should be given (e.g., Normally distributed errors).
- It should be clear whether the error bar is the standard deviation or the standard error of the mean.
- It is OK to report 1-sigma error bars, but one should state it. The authors should preferably report a 2-sigma error bar than state that they have a 96% CI, if the hypothesis of Normality of errors is not verified.
- For asymmetric distributions, the authors should be careful not to show in tables or figures symmetric error bars that would yield results that are out of range (e.g. negative error rates).
- If error bars are reported in tables or plots, The authors should explain in the text how they were calculated and reference the corresponding figures or tables in the text.

8. **Experiments compute resources**

   Question: For each experiment, does the paper provide sufficient information on the computer resources (type of compute workers, memory, time of execution) needed to reproduce the experiments?

   Answer: [Yes]

   Justification: Details on GPU resources and training time are provided in Section 5.1.

   Guidelines:

   - The answer NA means that the paper does not include experiments.
   - The paper should indicate the type of compute workers CPU or GPU, internal cluster, or cloud provider, including relevant memory and storage.
   - The paper should provide the amount of compute required for each of the individual experimental runs as well as estimate the total compute.
   - The paper should disclose whether the full research project required more compute than the experiments reported in the paper (e.g., preliminary or failed experiments that didn't make it into the paper).

9. **Code of ethics**

   Question: Does the research conducted in the paper conform, in every respect, with the NeurIPS Code of Ethics `https://neurips.cc/public/EthicsGuidelines`?

   Answer: [Yes]

   Justification: We have adhered strictly to the NeurIPS Code of Ethics in all our experiments.

   Guidelines:

   - The answer NA means that the authors have not reviewed the NeurIPS Code of Ethics.
   - If the authors answer No, they should explain the special circumstances that require a deviation from the Code of Ethics.
   - The authors should make sure to preserve anonymity (e.g., if there is a special consideration due to laws or regulations in their jurisdiction).

10. **Broader impacts**

    Question: Does the paper discuss both potential positive societal impacts and negative societal impacts of the work performed?

    Answer: [NA]

    Justification: This paper aims to advance the field of Machine Learning, particularly in training 3D reconstruction. We do not believe there are any specific societal consequences of our work that require special attention here.

    Guidelines:

    - The answer NA means that there is no societal impact of the work performed.

- If the authors answer NA or No, they should explain why their work has no societal impact or why the paper does not address societal impact.
- Examples of negative societal impacts include potential malicious or unintended uses (e.g., disinformation, generating fake profiles, surveillance), fairness considerations (e.g., deployment of technologies that could make decisions that unfairly impact specific groups), privacy considerations, and security considerations.
- The conference expects that many papers will be foundational research and not tied to particular applications, let alone deployments. However, if there is a direct path to any negative applications, the authors should point it out. For example, it is legitimate to point out that an improvement in the quality of generative models could be used to generate deepfakes for disinformation. On the other hand, it is not needed to point out that a generic algorithm for optimizing neural networks could enable people to train models that generate Deepfakes faster.
- The authors should consider possible harms that could arise when the technology is being used as intended and functioning correctly, harms that could arise when the technology is being used as intended but gives incorrect results, and harms following from (intentional or unintentional) misuse of the technology.
- If there are negative societal impacts, the authors could also discuss possible mitigation strategies (e.g., gated release of models, providing defenses in addition to attacks, mechanisms for monitoring misuse, mechanisms to monitor how a system learns from feedback over time, improving the efficiency and accessibility of ML).

11. **Safeguards**

    Question: Does the paper describe safeguards that have been put in place for responsible release of data or models that have a high risk for misuse (e.g., pretrained language models, image generators, or scraped datasets)?

    Answer: [NA]

    Justification: We believe our research, which focuses on 3D reconstruction, does not pose such risks.

    Guidelines:

    - The answer NA means that the paper poses no such risks.
    - Released models that have a high risk for misuse or dual-use should be released with necessary safeguards to allow for controlled use of the model, for example by requiring that users adhere to usage guidelines or restrictions to access the model or implementing safety filters.
    - Datasets that have been scraped from the Internet could pose safety risks. The authors should describe how they avoided releasing unsafe images.
    - We recognize that providing effective safeguards is challenging, and many papers do not require this, but we encourage authors to take this into account and make a best faith effort.

12. **Licenses for existing assets**

    Question: Are the creators or original owners of assets (e.g., code, data, models), used in the paper, properly credited and are the license and terms of use explicitly mentioned and properly respected?

    Answer: [Yes]

    Justification: All papers associated with the datasets we used have been properly cited.

    Guidelines:

    - The answer NA means that the paper does not use existing assets.
    - The authors should cite the original paper that produced the code package or dataset.
    - The authors should state which version of the asset is used and, if possible, include a URL.
    - The name of the license (e.g., CC-BY 4.0) should be included for each asset.
    - For scraped data from a particular source (e.g., website), the copyright and terms of service of that source should be provided.

- If assets are released, the license, copyright information, and terms of use in the package should be provided. For popular datasets, `paperswithcode.com/datasets` has curated licenses for some datasets. Their licensing guide can help determine the license of a dataset.
- For existing datasets that are re-packaged, both the original license and the license of the derived asset (if it has changed) should be provided.
- If this information is not available online, the authors are encouraged to reach out to the asset's creators.

13. **New assets**

    Question: Are new assets introduced in the paper well documented and is the documentation provided alongside the assets?

    Answer: [NA]

    Justification: We do not introduce any new assets in this paper.

    Guidelines:

    - The answer NA means that the paper does not release new assets.
    - Researchers should communicate the details of the dataset/code/model as part of their submissions via structured templates. This includes details about training, license, limitations, etc.
    - The paper should discuss whether and how consent was obtained from people whose asset is used.
    - At submission time, remember to anonymize your assets (if applicable). You can either create an anonymized URL or include an anonymized zip file.

14. **Crowdsourcing and research with human subjects**

    Question: For crowdsourcing experiments and research with human subjects, does the paper include the full text of instructions given to participants and screenshots, if applicable, as well as details about compensation (if any)?

    Answer: [NA]

    Justification: Our research does not involve crowdsourcing nor research with human subjects.1080

    Guidelines:

    - The answer NA means that the paper does not involve crowdsourcing nor research with human subjects.
    - Including this information in the supplemental material is fine, but if the main contribution of the paper involves human subjects, then as much detail as possible should be included in the main paper.
    - According to the NeurIPS Code of Ethics, workers involved in data collection, curation, or other labor should be paid at least the minimum wage in the country of the data collector.

15. **Institutional review board (IRB) approvals or equivalent for research with human subjects**

    Question: Does the paper describe potential risks incurred by study participants, whether such risks were disclosed to the subjects, and whether Institutional Review Board (IRB) approvals (or an equivalent approval/review based on the requirements of your country or institution) were obtained?

    Answer: [NA]

    Justification: Our research does not involve crowdsourcing nor research with human subjects.1080

    Guidelines:

    - The answer NA means that the paper does not involve crowdsourcing nor research with human subjects.

- Depending on the country in which research is conducted, IRB approval (or equivalent) may be required for any human subjects research. If you obtained IRB approval, you should clearly state this in the paper.
- We recognize that the procedures for this may vary significantly between institutions and locations, and we expect authors to adhere to the NeurIPS Code of Ethics and the guidelines for their institution.
- For initial submissions, do not include any information that would break anonymity (if applicable), such as the institution conducting the review.

16. **Declaration of LLM usage**

    Question: Does the paper describe the usage of LLMs if it is an important, original, or non-standard component of the core methods in this research? Note that if the LLM is used only for writing, editing, or formatting purposes and does not impact the core methodology, scientific rigorousness, or originality of the research, declaration is not required.

    Answer: [NA]

    Justification: We use LLM for editing (e.g., grammar, spelling, word choice).

    Guidelines:

    - The answer NA means that the core method development in this research does not involve LLMs as any important, original, or non-standard components.
    - Please refer to our LLM policy (`https://neurips.cc/Conferences/2025/LLM`) for what should or should not be described.